Rare-Earth Surface Alloying: A New Phase for $GdAu_2$

M. Corso,[1] M. J. Verstraete,[1,2] F. Schiller,[1] M. Ormaza,[3] L. Fernández,[1] T. Greber,[5] M. Torrent,[6] A. Rubio,[1,2,4] and J. E. Ortega[1,3]

[1]*DIPC and Centro de Física de Materiales (CSIC-UPV/EHU), E-20018 San Sebastián, Spain*
[2]*ETSF and Nano-bio Spectroscopy Group (UPV/EHU), E-20018 San Sebastián, Spain*
[3]*Departamento de Física Aplicada I (UPV/EHU), E-20018 San Sebastián, Spain*
[4]*Fritz-Haber-Institut der Max-Planck-Gesellschaft, D-14195 Berlin, Germany*
[5]*Physics Institute, University of Zurich, CH-8057 Zurich, Switzerland*
[6]*CEA, DAM, DIF, F-91297, Arpajon, France*

(Received 7 April 2010; published 2 July 2010)

Surface alloying is a powerful way of varying physical and chemical properties of metals, for a number of applications from catalysis to nuclear and green technologies. Surfaces offer many degrees of freedom, giving rise to new phases that do not have a bulk counterpart. However, the atomic characterization of distinct surface compounds is a major task, which demands powerful experimental and theoretical tools. Here we illustrate the process for the case of a $GdAu_2$ surface phase of extraordinary crystallinity. The combined use of surface-sensitive techniques and state-of-the-art *ab initio* calculations disentangles its atomic and electronic properties. In particular, the stacking of the surface layers allows for gadolinium's natural ferromagnetic state, at variance with the bulk phase, where frustration leads to antiferromagnetic interlayer coupling.

DOI: 10.1103/PhysRevLett.105.016101 PACS numbers: 68.55.−a, 68.35.−p, 73.61.At, 81.05.Bx

Many of the greenest technologies of the age, from electric cars to efficient light bulbs to very large wind turbines and future magnetic refrigeration, are made possible by an unusual group of elements: the rare earths (REs). The rare earths possess exotic electronic structure and delicately changing bonding, due to the presence of shallow and interacting d- and f-electron levels. These electrons are responsible for high and specific catalytic activities [1], remarkable alloying in metals [2], and specific luminescent properties [3]. Precisely this richness, and the associated complexity, makes the determination of the structure and properties of RE materials very challenging. The REs demonstrate varying magnetism, coordination, oxidation states, and bonding types, as a function of the number and localization of the f-band electrons. A striking example is cerium, whose isostructural volume-collapse transition is still not fully explained [4,5]. All of these properties correspond to and explain the chemical reactivity, tunable optical response, and alloying behavior of the REs and their compounds. The past decade has seen a further revival of RE physics and chemistry, thanks to their interaction with nanostructuring: the specific electronic behavior of the REs can be combined with nanoscopic confinement and energy level discretization [3], for example, to enhance thermoelectrical efficiency [6]. In bulk and nanostructures, the REs are at the crux of strongly correlated and heavy-fermion physics [7,8], giving rise to Kondo physics, a mix of magnetism, alloying, and localization-delocalization transitions.

Prototypical and extremely rich RE systems are created by the alloying of gadolinium with d-band metals, and, in particular, gold and silver. These systems present magnetism, Kondo phenomena, and crystal structures which are tunable depending on the precise alloy and on the RE content. Gadolinium is a borderline rare earth, which is naturally ferromagnetic but can easily switch to different magnetic states depending on the coordination (surface and cluster structure) [9]. Surface alloying introduces further degrees of freedom, and can give rise to novel phases. Here we study a new surface compound created by reactive epitaxy of Gd on a Au(111) crystal. Angle-resolved and core-level photoemission (ARPES, XPS) and scanning tunneling microscopy (STM) demonstrate that a layer-by-layer growth of a stoichiometric $GdAu_2$ alloy occurs under particular conditions of Gd vapor flux and substrate temperature. Our theoretical analysis determines a particular layer stacking and magnetic ordering, at variance with bulk $GdAu_2$ crystals [10,11]. Moreover, the experiment and theory feedback allows the characterization of the nature of electron bands, and, in particular, explains the exotic tip-height-dependent image contrast observed in STM.

Reactive growth of Gd on Au(111) is carried out by exposing the Au(111) surface, held at 550 K, to a pure Gd vapor. This procedure leads to alloyed Au-Gd surface structures, which depend on the Gd coverage fraction [12,13]. In the submonolayer range one can observe the smooth transformation of the Au-herringbone reconstruction into a network of *trigons*, followed by homogeneous nucleation of one monolayer (ML) thick $GdAu_2$ islands. The latter show atomic perfection and a particularly attractive moiré pattern, which arises due to the lattice mismatch with the underlying Au substrate [12,13]. A second layer grows in a layer-by-layer fashion, as demonstrated in this

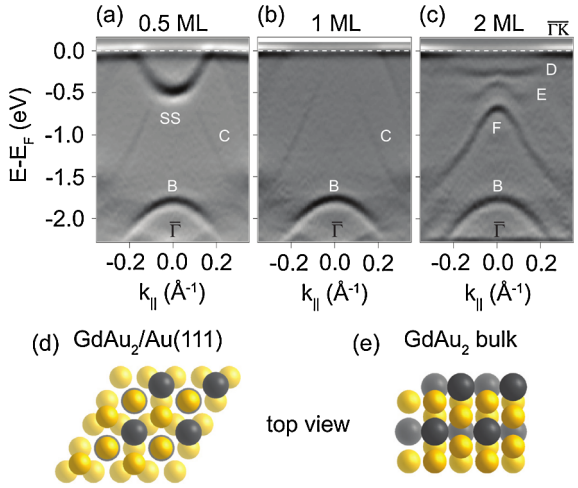

FIG. 1 (color online). (a–c) Second derivative dispersion plots of the photoemission intensities corresponding to different Gd-Au sample preparations: (a) 0.5 ML $GdAu_2$/Au(111), (b) 1 ML $GdAu_2$/Au(111), and (c) 2 ML $GdAu_2$/Au(111). The $\overline{\Gamma K}$ direction refers to the first Brillouin zone of the $GdAu_2$ surface (further details in supplementary material [15]). (d) Top view of the $GdAu_2$ bilayer, as determined in density functional theory. (e) Same for two (110) layers of bulk tetragonal $GdAu_2$.

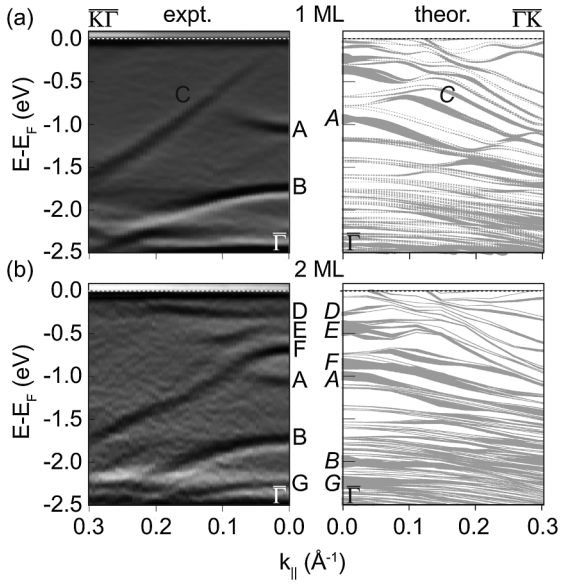

FIG. 2. (a) Left: ARPES measurement of the single monolayer compound electronic structure (left) measured at $h\nu = 36.2$ eV along the $\overline{\Gamma K}$ direction. Right: corresponding theoretical band structure. (b) Left: the same ARPES measurement taken at $h\nu = 33.2$ eV for a $GdAu_2$ bilayer on Au(111) and its corresponding theoretical band structure (right). Labels *A*–*G* indicate the different bands observed in the experiment and the corresponding calculated ones.

Letter. The ARPES data of Figs. 1(a) and 1(c) show electronic bands for a Au(111) sample covered by $GdAu_2$ islands one layer thick [Fig. 1(a)], by a full $GdAu_2$ monolayer [Fig. 1(b)], and finally by a $GdAu_2$ bilayer [Fig. 1(c)]. A sharp transition from 1 ML to 2 ML is observed, reflecting the layered structure of the $GdAu_2$ surface compound. The topmost surface layer geometry was probed with STM, and corresponds to an expanded $GdAu_2$(110) plane [12,13]. However, the bilayer packing is different from that of bulk $GdAu_2$, as depicted in Figs. 1(d) and 1(e). The $GdAu_2$/Au(111) bilayer structure has been determined with diffraction data and theoretical calculations. The changing distance between the Gd atoms induces a change in the sign of the spin coupling [from antiferromagnetic (AFM) in the bulk to ferromagnetic (FM) in the surface alloy], following an RKKY-type interaction [14].

Surface bands in Fig. 1 are measured around the $\bar{\Gamma}$ point in the first surface Brillouin zone by ARPES, using 44 eV photons at the Synchrotron Radiation Center (SRC) in Stoughton, Wisconsin (see supplementary material [15]). Measurements are carried out at 150 K. The partially covered substrate [Fig. 1(a)] is characterized by the presence of both the Au surface state [marked as SS in Fig. 1(a)], whose position is unchanged with respect to that of clean Au(111), and the 1 ML thick $GdAu_2$ compound bands. The Au surface state disappears when the surface is fully covered in Fig. 1(b), and only the $GdAu_2$ bands remain. One can discriminate three bands, namely, *A*, dispersing upwards from $\overline{\Gamma K}$ (better observed at 33.2 eV in Fig. 2), and *B* and *C*, dispersing downwards. When the Gd content is further increased, three new bands (*D*, *E*, *F*) are added, closer to E_F. The 2:1 stoichiometry in Figs. 1(b) and 1(c) is confirmed by Au and Gd 4*f* intensities from pure Au(111) and a thick layer of $GdAu_2$ [13], but mainly by the STM tip-surface distance contrast shown in Fig. 4 and discussed below. We conclude that bands shown in Figs. 1(b) and 1(c) correspond to one and two layers of $GdAu_2$.

The nature of the bands with ARPES can be appropriately determined with first-principles calculations, which additionally allows us to test the particular layer stacking in the 2 ML film (we use density functional theory—see supplementary material [15]). A (2×2) supercell of the Au (111) surface is constructed, on which the different overlayers are deposited. The optimized atomic structure resulting from our calculations, for the double layer compound, consists of two $GdAu_2$ layers shifted one with respect to the other, in such a way that each Gd atom in one layer corresponds to a Au atom in the other layer ([Fig. 1(d)]. This packing differs from the bulk termination as seen in Figs. 1(d) and 1(e). The relaxed surface layers show a total surface corrugation of 0.34 Å (distinct from the moiré pattern). Atomic heights $h = z_{\text{atom}} - z_{\text{Gd}}$ are given relative to the sublayer Gd. Three inequivalent atoms coexist in the surface: (1) Au atoms (Au_1) placed above Gd, pushed outwards to $h = 2.74$ Å, (2) Gd atoms sitting on top of Au atoms, which are a bit lower ($h = 2.44$ Å), and (3) Au atoms (Au_2) on top of another Au, with $h = 2.40$ Å. The presence of three inequivalent surface atoms is further proven in STM below. On the other hand, all structures are tested in FM and AFM configurations for

the f-electron densities on the gadolinium. In the bilayer structures the *ferro*magnetic configuration is preferred in all cases. This can be linked to the different Au-Gd layer stacking. The Au coordination decreases from 10 to 7 or 8 (six in-plane plus one or two vertical neighbors). The Gd-Gd distance decreases from 5.2 to 4.12 Å, and the AFM coupling becomes FM (bulk Gd is FM).

In Fig. 2 we compare the theoretical and ARPES electronic structures of the 1 and 2 ML alloys. To estimate the visibility of each electronic band in ARPES, the $m = 0$ angular momentum character of the bands (for all l) is shown as the band width in Fig. 2. The correspondence between theoretical and ARPES bands is quite good, given a possible small shift in the Fermi level due to the finite size of the slab system, the imposed commensurability of the alloy and Au layers (which strains the alloy), and many-body effects which should increase the band widths slightly. Of particular note in the 2 ML case are the doubling of the C band, and the flatness of the D band just below E_F. The assignment of the bands to atomic character is straightforward: the manifold below 2 eV (bands B and G) is the Au-d band. The flat band labeled D is of Gd-d character—the corresponding bands in the 1 ML case are unoccupied due to charge transfer from Gd to Au. Finally, the surface bands (A, E, F) are hybridized Au-s and Gd-d states, with contributions from both $GdAu_2$ layers in the 2 ML case. In particular the upwards dispersing s-like A band appears as a succession of anticrossings in the calculation.

The particular stacking of the bilayer $GdAu_2$ compound is confirmed by x-ray photoelectron diffraction (XPD) experiments (see also supplementary material [15]). The Gd $3d_{5/2}$ XPD pattern, measured with Si K-α at a kinetic energy of $E_{\mathrm{kin}} = 553$ eV, is shown in Fig. 3(a). To a first approximation this pattern can be interpreted as a forward projected image of the atomic surrounding of photoemitting Gd atoms in the compound. The experimental pattern is dominated by seven intense forward-scattering peaks [Fig. 3(a)], which are a clear evidence for the existence of a second $GdAu_2$ layer. The central peak ([111] direction) demonstrates the on-top stacking shown in Fig. 1(d), and excludes the natural bulk stacking [Fig. 1(e)]. The other six forward-scattering maxima spaced by 60° in azimuth, at a polar angle of 56° ± 0.5°, are due to forward scattering of photoelectrons emitted by Gd atoms below the surface layer. Considering that nearest neighbors are separated by an in-plane distance of 5.5 ± 0.3 Å, Gd emitters must be ~2.2 Å below the surface atoms. The theoretical relaxations give alloy layers with each Gd paired to a Au and not a Gd in the other layer (Fig. 1—this cannot be easily distinguished from XPD). The 2.2 Å agree well with the theoretical distance of ~2.4 Å. Finally, the Gd $3d_{5/2}$ XPD pattern is simulated with the electron diffraction in atomic clusters multiple scattering calculation software [16]. The relaxed *ab initio* positions are used (in the case of commensurability with the substrate), and the two possible 60° rotated orientations of the surface layer are considered. The final pattern, which best fits the XPD data [Fig. 3(b)], results from the sum of four XPD patterns calculated for Gd emitters in the two layers of each of two equivalent domains, rotated 60° one with respect to the other.

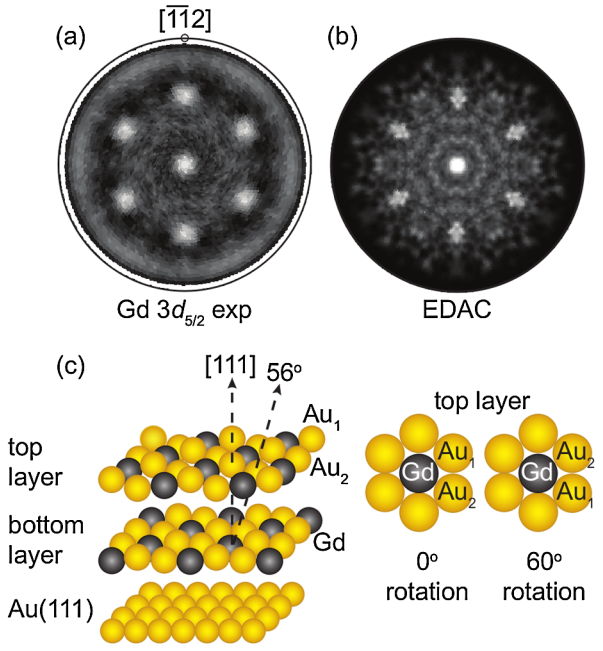

FIG. 3 (color online). (a) X-ray photoelectron diffraction pattern recorded at the Gd $3d_{5/2}$ emission ($E_{\mathrm{kin}} = 553$ eV) for the 2 ML $GdAu_2$/Au(111) compound. (b) Multiple scattering calculation for the pattern in (a), simulated with the electron diffraction in atomic clusters (EDAC) code [16]. The total pattern in (b) results from the sum of 4 multiple scattering calculations for Gd atoms in the top and bottom $GdAu_2$ layers when the top layer is 0° or 60° degrees rotated to the bottom one as schematically pictured in (c).

Final proof of the bilayer stacking and stoichiometry comes from the singular tip-height dependence observed in STM images. By tuning the tunneling current (I_T), and therefore the tip-sample distance, we are able to image the three inequivalent atoms on the surface predicted by the theoretical calculation. Increasing the current [Figs. 4(a)–4(c)], the images go from a hexagonal lattice of holes, to one of protrusions, and to a mixed case, with one intense and one weak protrusion. Such an effect is explainable by the STM tip selectively detecting different electronic states at different heights. The STM images are calculated *ab initio* using the Tersoff-Hamann scheme [17], and explain the differences observed for a fixed surface topology and bias. For a voltage of $V = -1.2$ V, the STM current density is plotted on the right of Figs. 4(d)–4(f) for different values of the partial density of states. As a function of current, the tip lies at different distances above the surface, from 5.19 down to 2.23 Å. At large distances, the Gd and Au_2 atoms are visible, in an intermediate range only the Au_1 atoms appear, and close to

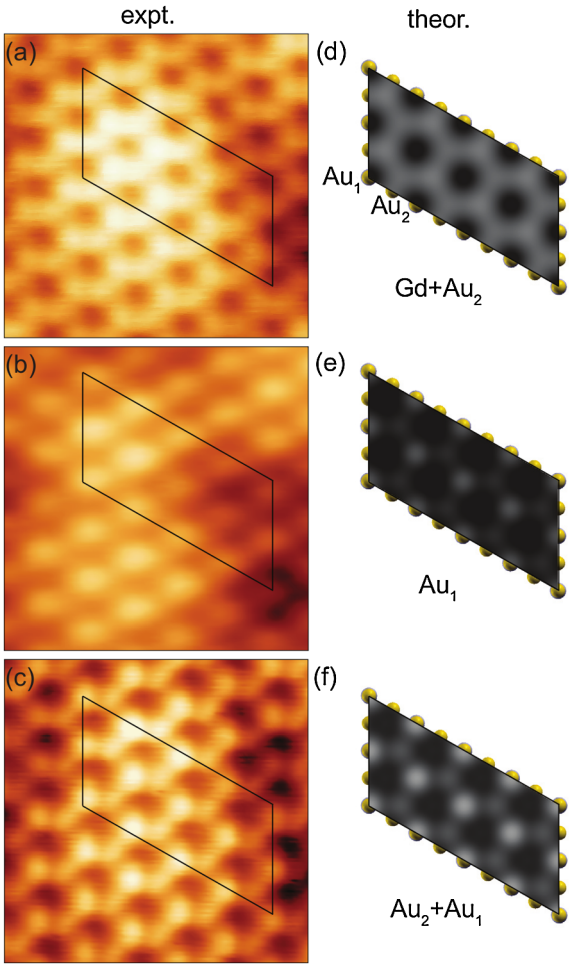

FIG. 4 (color online). (a–c) High resolution STM images of the bilayer $GdAu_2$ surface compound, grown on Au(111). Three different atomic contrasts are measured by fixing the sample bias voltage (V_S) and tuning the tunneling current (I_T): (a) $I_T = 0.3$ nA, $V_S = -1.2$ V; (b) $I_T = 1$ nA, $V_S = -1.2$ V; (c) $I_T = 2$ nA, $V_S = -1$ V. (d, e) Theoretical calculations allowing us to identify the different atomic species visible in (a–c) as indicated. Simulations are done at $V_S = -1.2$ V and decreasing STM tip-sample distance (d_{TS}) from $d_{TS} = 5.19$ Å in (d), to $d_{TS} = 2.61$ Å in (e), and to $d_{TS} = 2.23$ Å in (f).

the surface the two Au atoms (inequivalent, due to the sublayer) are visible with different intensities. This inversion of contrasts in STM images at constant bias is rare, but can be understood in light of the bilayer band structure of Fig. 2: at $V = -1.2$ eV bias one is actually probing all electronic states spanning from -1.2 eV up to the Fermi energy. This range comprises the complex hybrid s-d levels, which have different extents at the Au and Gd sites.

In summary, we have shown that the unambiguous determination of the electronic and structural properties of surface phases in alloys requires the combination of cutting-edge surface-sensitive experimental techniques with first-principles modeling. The new stacking sequence found for $GdAu_2$ allows gadolinium's natural ferromagnetic state, in contrast to bulk $GdAu_2$. Our results would be relevant to explaining the properties of other f-metal complexes.

We thank B. Amadon for the Gd potential. We acknowledge support from the Belgian FNRS, EU FP7 project "THEMA" (G.A. 228539), ACI-Promociona (ACI2009-1036), iNanogune ETORTEK, and the EU FP7 "ETSF I3" project (G.A. 211956). Computer time was provided by the Red Española de Supercomputacion and ARINA (UPV/EHU). This work was supported in part by the Spanish MICINN (FIS2007-65702-C02-01 and MAT2007-63083) and the Basque Government (IT-257-07 and IT-319-07). The SRC is supported by the NSF under Grant No. DMR-0537588.

[1] T. Mashiko, N. Kumagai, and M. Shibasaki, J. Am. Chem. Soc. **131**, 14 990 (2009).
[2] G. M. Müller *et al.*, Nature Mater. **8**, 56 (2009).
[3] S. Schietinger, L. de S. Menezes , B. Lauritzen, and B. Oliver, Nano Lett. **9**, 2477 (2009).
[4] G. Kotliar, S. Savrasov, K. Haule, V. Oudovenko, O. Parcollet, and C. Marianetti, Rev. Mod. Phys. **78**, 865 (2006).
[5] B. Amadon, S. Biermann, A. Georges, and F. Aryasetiawan, Phys. Rev. Lett. **96**, 066402 (2006).
[6] J. P. Heremans, V. Jovovic, E. S. Toberer, A. Saramat, K. Kurosaki, A. Charoenphakdee, S. Yamanaka, and G. J. Snyder, Science **321**, 554 (2008).
[7] A. Schröder, G. Aeppli, R. Coldea, M. Adams, O. Stockert, H. Löhneysen, E. Bucher, R. Ramazashvili, and P. Coleman, Nature (London) **407**, 351 (2000).
[8] Y.-F. Yang, Z. Fisk, H.-O. Lee, J. Thompson, and D. Pines, Nature (London) **454**, 611 (2008).
[9] B. Koopmans, G. Malinowski, F. Dalla Longa, D. Steiauf, M. Fähnle, T. Roth, M. Cinchetti, and M. Aeschlimann, Nature Mater. **9**, 259 (2009).
[10] A. Saccone, M. L. Fornasini, D. Macciò, and S. Delfino, Intermetallics **4**, 111 (1996).
[11] L. Tung, K. Buschow, J. Franse, and N. Thuy, J. Magn. Magn. Mater. **154**, 96 (1996).
[12] L. Fernández, M. Corso, F. Schiller, M. Ilyn, M. Holder, and J. Ortega, Appl. Phys. Lett. **96**, 013 107 (2010).
[13] M. Corso, L. Fernández, F. Schiller, and J. E. Ortega, ACS Nano **4**, 1603 (2010).
[14] T. Kasuya, Prog. Theor. Phys. **16**, 45 (1956).
[15] See supplementary material at http://link.aps.org/supplemental/10.1103/PhysRevLett.105.016101 for technical details on ARPES, XPD, and STM experiments, EDAC simulations, and theoretical calculations.
[16] F. J. García de Abajo, M. A. Van Hove, and C. S. Fadley, Phys. Rev. B **63**, 075404 (2001).
[17] J. Tersoff and D. R. Hamann, Phys. Rev. Lett. **50**, 1998 (1983).